

# Workspace Analysis of a Floating Multi-Robot Coordinated Lifting System

Cheng Su<sup>1</sup>, Xiangtang Zhao<sup>1</sup>, Zengzhen Yan<sup>1</sup>, Zhigang Zhao<sup>1</sup> and Jiadong Meng<sup>1</sup>

Received: 25 October 2022 / Accepted: 30 May 2023  
© Harbin Engineering University and Springer-Verlag GmbH Germany, part of Springer Nature 2024

## Abstract

At present, the cranes used at sea have several shortcomings in terms of flexibility, efficiency, and safety. Therefore, a floating multi-robot coordinated lifting system is proposed to fulfill the offshore lifting requirements. First, the structure of the lifting system is established according to the lifting task, the kinematic model of the system is developed by using the D–H coordinate transformation, and the dynamic model is developed based on rigid-body dynamics and hydrodynamics. Then, the static and dynamic workspace of the lifting system are analyzed, and the solving steps of the workspace are given by using the Monte–Carlo method. The effect of the load mass and the maximum allowable tension of the cable on the workspace is examined by simulation. Results show that the lifting system has limited carrying capacity and a data reference for selecting the structural parameters by analyzing the factors affecting the workspace. Findings provide a basis for further research on the optimal design of structural parameters and the determination of safe configurations of the lifting system.

**Keywords** Offshore lifting; Multi-robot system; Kinematic model; Dynamic model; Static workspace; Dynamic workspace

## 1 Introduction

With the development of science and technology, humans have gradually deepened their exploration of the oceans. At present, all countries use a single crane for lifting operations. With the development of marine engineering, traditional cranes can no longer meet the current demand for efficiency, load capacity, and safety of lifting equipment (Jia et al., 2015; Qian et al., 2017; Liu et al., 2021a). These problems are solved by adopting the coordinated tasks of multiple lifting equipment, which can increase the stability of the lifting system, reduce the working load of single lifting equipment, and improve safety (Ding et al., 2012; Qian et al., 2014; Wang et al., 2012).

The lifting system combines the advantages of a multi-robot lifting system and a traditional lifting ship. Such advantages include high bearing capacity, large workspace, high stability, and capacity to meet the lifting operation under

complex maritime environments (Chen et al., 2001; Su et al., 2021). Thus, the lifting system has high research and practical values. Scholars have studied this field and attained several achievements. Yu et al. (2021, 2022) proposed a hybrid framework using visual and force sensing for human–robot co-carrying tasks, and an adaptive impedance controller for human–robot co-transportation was put forward in task space; the performance of the proposed techniques is shown using simulations and experiments. Horoub et al. (2017, 2018) established the dynamic equation of the hoisting device at sea and determined the cable tension and the workspace of the hoisting object. Chen et al. (2020) developed a cable-driven lifting device that used the cable and the motor drive to realize the pose and position movements of the load, respectively. Ren et al. (2008) established a nonlinear dynamic model of the floating cranes to simulate the influence of waves. Idres et al. (2003) established a crane model under eight degrees of freedom (DOF) and analyzed the unidirectional coupled motion between load and hull. Cong et al. (2005) established a dynamic equation of the cable traction robot. Bedoustani et al. (2009) considered the elasticity of the cable-driven parallel manipulator and established a dynamic model. The shape and size of the workspace are important indexes for analyzing the performance and stability of the lifting system (Li, 2021). Verhoeven and Hiller (2000) estimated the workspace of the tendon platform using algebraic sets. Bosscher et al. (2006) used vector theory to solve the analytical solution of the workspace of a cable-driven parallel robot and discussed the possibility of solving the workspace boundary. Diao and

### Article Highlights

- The workspace of the lifting system is divided into static and dynamic workspaces.
- The effect of load mass and the maximum allowable cable tension on the workspace are analyzed.
- The lifting system has a data reference for selecting the structural parameters by analyzing the factors affecting the workspace.

✉ Zhigang Zhao  
zhaozhg@mail.lzjtu.cn

<sup>1</sup> Department of Mechanical Engineering, Lanzhou Jiaotong University, Lanzhou 730070, China

Ou (2007) solved the workspace of a parallel robot under complete constraints according to the vector closure principle. Guan and Yokoi (2006) used the Monte–Carlo algorithm to analyze the reachable workspace of humanoid robots. These previous studies focused on fully and over-constrained systems. Under-constrained systems do not satisfy the force-spinor closure condition (Tang et al., 2013; Liu et al., 2021b) and thus have few research results. In this study, the workspace of the lifting system is divided into static and dynamic workspaces.

The floating multi-robot coordinated lifting system is an under-constrained system. In preliminary research, using real objects is dangerous. Therefore, theoretical analysis and simulations of the lifting system are necessary (Bisgaard et al., 2009; Bendtsen et al., 2010). Based on the lifting task, the spatial configuration of the lifting system was designed, the kinematic model of the system was established by using the D–H coordinate transformation, and the dynamic model was developed based on rigid-body dynamics and hydrodynamics, and the constraints that the load position must satisfy were obtained. Then, the workspace of the lifting system is divided into static and dynamic workspaces, and based on the virtual cable and the closed principle of force-spinor, the calculated steps of the workspace of the lifting system are obtained by the Monte–Carlo algorithm. The influence of load mass and maximum allowable tension of cables on static and dynamic workspaces are analyzed. As a new research direction, the workspace of the lifting system is the focus of this study. The lifting system has a data reference for selecting the structural parameters by analyzing the factors affecting the workspace, which provides guidance for practical applications.

## 2 Kinematic analysis of the system

The lifting system consists of the floating robot and the cable-driven parallel lifting system. Figure 1 shows the structure. In the floating robot, the lower half is a floating base, and the upper half is a three-DOF joint manipulator. Link 1 can rotate around the Z-axis, and links 2 and 3 can rotate in the same vertical plane. The coordinate system  $\{O\}$  is set in the horizontal plane,  $\{O_i\}$  is set at the barycenter of the floating base,  $\{O_{si}\}$  is set at the bottom of the robot, and  $\{O'\}$  is set at the center of the load. In this coordinate system,  $A_i$  denotes the robot endpoints,  $B_i$  denotes the connection points between the cables and the load,  $L_i$  denotes the cables, and  $r(x, y, z, \varphi_1, \varphi_2, \varphi_3)$  denotes the position and pose of the load. The rod length of the robot is  $(a_{i1}, a_{i2}, a_{i3})$ , and the joint angle is  $(\theta_{i1}, \theta_{i2}, \theta_{i3})$ . Given that the whole system is composed of three lifting robots, then  $i=1, 2, 3$ . The load moves according to the desired trajectory by adjusting the position of the robot end or the cable length, and the cable is adjusted by the actuator at the robot end.

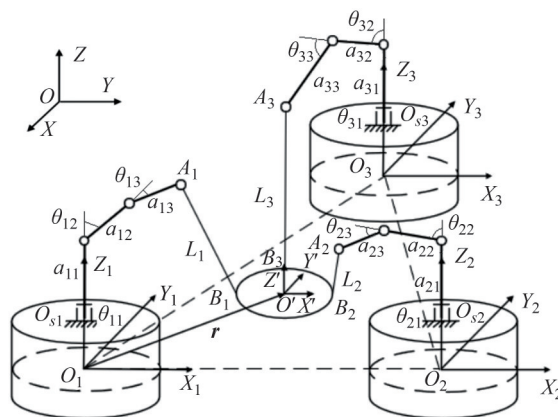


Figure 1 Structure of a lifting system with a floating base

Given the complex structure of the actual lifting system, the following assumptions are made in the analysis without affecting its results.

- 1) The robots are evenly distributed, the ends of the lifting robots do not overlap, and the cables do not intertwine.
- 2) The floating base is a rigid body with uniform mass. The waves acting on the floating base are linearly regular, and the coupling between the DOF of the floating base is not considered.
- 3) The structural stiffness of the robot is strong enough to ignore the elastic vibration and deformation of the robot under force. When the cable is stressed, it is treated as a rigid body, and its elastic deformation and mass are ignored.
- 4) The floating robot is regarded as the ideal working state, and the influence of its internal forces generated on the floating base and lifting system is temporarily neglected.

### 2.1 Kinematic analysis of floating robot

Assuming that the three floating robots have the same structures, the end coordinates of the lifting robot can be obtained in the coordinate system  $\{O_{si}\}$ :

$$\begin{bmatrix} x_{Ai}^* \\ y_{Ai}^* \\ z_{Ai}^* \\ 1 \end{bmatrix} = \begin{bmatrix} a_{i3}c\theta_{i1}c\theta_{i2}c\theta_{i3} - a_{i3}c\theta_{i1}s\theta_{i2}s\theta_{i3} + a_{i2}c\theta_{i1}c\theta_{i2} \\ a_{i3}s\theta_{i1}c\theta_{i2}c\theta_{i3} - a_{i3}s\theta_{i1}s\theta_{i2}s\theta_{i3} + a_{i2}s\theta_{i1}c\theta_{i2} \\ a_{i1} + a_{i2}s\theta_{i2} + a_{i3}c\theta_{i2}s\theta_{i3} + a_{i3}s\theta_{i2}c\theta_{i3} \\ 1 \end{bmatrix} \quad (1)$$

where  $s$  is  $\sin$ ,  $c$  is  $\cos$ .

From the structure of the floating robot and the related theory of robot kinematics, the end position of the lifting robot is  $(x_{Ai}, y_{Ai}, z_{Ai}, 1)$ :

$$\begin{bmatrix} x_{Ai} \\ y_{Ai} \\ z_{Ai} \\ 1 \end{bmatrix} = \mathbf{R}^* \mathbf{R} \begin{bmatrix} x_{Ai}^* \\ y_{Ai}^* \\ z_{Ai}^* \\ 1 \end{bmatrix} \quad (2)$$

where  $\mathbf{R}^*$  is the transformation matrix between coordinate systems  $\{O_i\}$  and  $\{O_{si}\}$ , obtained by

$$\mathbf{R}^* = \begin{bmatrix} \cos\varphi_i & -\sin\varphi_i & 0 & x_i \\ \sin\varphi_i & \cos\varphi_i & 0 & y_i \\ 0 & 0 & 1 & z_i \\ 0 & 0 & 0 & 1 \end{bmatrix}$$

where the position of the origin  $O_{si}$  of  $\{O_{si}\}$  in  $\{O_i\}$  is  $(x_i, y_i, z_i)$ , and the angle of  $\{O_{si}\}$  relative to  $\{O_i\}$  is  $\varphi_i$ .

In Equation (2),  $\mathbf{R}$  is the transformation matrix between  $\{O_i\}$  and  $\{O\}$ .

$$\mathbf{R} = \begin{bmatrix} c\beta_i c\gamma_i & -c\beta_i s\gamma_i & s\beta_i & x_{si} \\ c\alpha_i s\gamma_i + s\alpha_i s\beta_i c\gamma_i & c\alpha_i c\gamma_i - s\alpha_i s\beta_i s\gamma_i & -s\alpha_i c\beta_i & y_{si} \\ s\alpha_i s\gamma_i - c\alpha_i s\beta_i c\gamma_i & s\alpha_i c\gamma_i + c\alpha_i s\beta_i s\gamma_i & c\alpha_i c\beta_i & z_{si} \\ 0 & 0 & 0 & 1 \end{bmatrix}$$

where angles  $(\alpha_i, \beta_i, \gamma_i)$  of the floating base around the three axes indicate its roll, pitch, and heave motion, respectively; the positions  $(x_{si}, y_{si}, z_{si})$  of the floating base in space indicate its lateral, longitudinal, and vertical motions.

The kinematic relationships between the end of the lifting robot and the floating base can be obtained by Equations (1) and (2).

## 2.2 Kinematic analysis of the lifting system

The connection points between the load and the cables are  $B_i'$  in  $\{O'\}$ .

$$\mathbf{B}_i = \mathbf{R}_G \mathbf{B}_i' + \mathbf{r} \quad (3)$$

where  $\mathbf{R}_G$  is the transformation matrix of  $\{O'\}$  relative to  $\{O\}$  (Craig et al., 2018).

From the coordinates of  $A_i$  and  $B_i$ , the cable length can be obtained as follows.

$$L_i = \sqrt{(x_{Ai} - x_{Bi})^2 + (y_{Ai} - y_{Bi})^2 + (z_{Ai} - z_{Bi})^2} \quad (4)$$

According to the motion law of the floating base and the robot, the end coordinates of the lifting robot, cable length, coordinates of the connection point between the load and cable, and the load position can be obtained by connecting Equations (1) to (4).

The load workspace can be obtained by considering the geometric constraints of the lifting system during the kinematic solution.

1) The load position is always in the triangular prism formed by the end points of the three robots and their projection points on the horizontal plane.

2) The pose of the load must be less than a certain angle to avoid the unbalanced distribution of the cable tension.

3) The cable tension must be between the minimum pre-load force and the maximum allowable tension to avoid the virtual strain and fracture of the cable.

4) For the floating base, its draft depth is less than its height to ensure that it will not be submerged in water.

## 3 Dynamic analysis of the system

The floating multi-robot coordinated lifting system consists of two parts: a cable-driven parallel lifting system and floating robots. The dynamic equations of the floating robot and the cable-driven parallel lifting system are established separately, and the dynamic model of the whole lifting system is simultaneously obtained.

### 3.1 Dynamic analysis of floating robot

The floating robot consists of a joint robot fixed on a floating base. In the analysis of its dynamics, these two parts are considered as the same rigid body, and the effect of the robot's pose on the floating base is neglected.

According to the idea of separation modeling (Schellin et al., 1991), the motion equation of the floating robot in the heaving direction under the action of external forces such as from waves (wave excitation and radiation forces), restoration, and damping is established as

$$\mathbf{M}_z z'' + 2\mathbf{N}_z z' + \mathbf{C}_z z = \mathbf{F}_z + \mathbf{T}_z \quad (5)$$

where  $z''$  is the acceleration of the floating robot along the  $Z$  direction,  $\mathbf{M}_z = m_G + \lambda_z$  is the inertia moment,  $\mathbf{N}_z$  is the damping moment,  $\mathbf{C}_z = \rho S_w$  is the recovery moment,  $m_G$  is the mass matrix of the floating robot,  $\lambda_z$  is the additional mass matrix,  $\rho$  is the fluid density,  $S_w$  is the area of the water plane,  $\mathbf{F}_z$  is the wave disturbance torque, and  $\mathbf{T}_z$  is the in  $Z$  direction torque of the cable tension of the floating robot. The coefficients in the motion equations of the floating robot can be obtained by referring to that of the crane ship.

### 3.2 Dynamic analysis of the lifting system

In the process of starting and braking the multi-robot coordinated lifting system, the load swings because the dynamic balance condition is damaged by its inertial force. The movement of the floating base transfers to the end of the robot, causing a large swing of the load. Even without any external disturbance, the load inevitably swings when the floating robot adjusts the joint angle. Due to the uncertainty in the direction of the load motion of the lifting system, it is analyzed as a spherical pendulum process to facilitate the derivation of the dynamical model. Figure 2 shows the structure diagram of the lifting system, where  $A$  denotes the end point of the lifting robot,  $Q$  denotes the load,  $l$  is the cable length, and  $m$  is the load mass. Assuming that the cable force is  $T$ , the mass and deformation of the cable are not considered in the dynamic analysis, and the direction of the force is always along the direction of the cable tension.

The in- and out-plane angles  $\theta_x$  and  $\theta_y$  are used to locate the position of the cable in the lifting system. Assuming that the cable is parallel to the  $Z$ -axis in the initial state, it rotates a degree  $\theta_x$  during the load movement from state 1 to 2. When the load moves from state 2 to 3, the cable rotates by

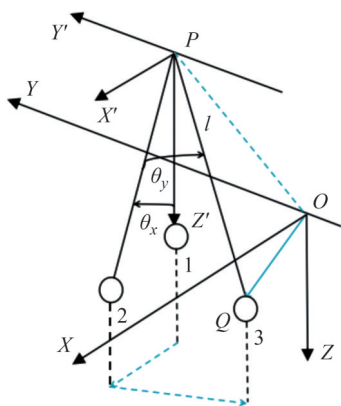


**Figure 2** Diagram of the lifting system

a degree of  $\theta_y$ . Then, the position of the load is denoted as:

$$\begin{cases} x_q(t) = x_p(t) + l(t) \cdot \sin\theta_x(t) \cos\theta_y(t) \\ y_q(t) = y_p(t) - l(t) \cdot \sin\theta_y(t) \\ z_q(t) = z_p(t) + l(t) \cdot \cos\theta_x(t) \cos\theta_y(t) \end{cases} \quad (6)$$

The dynamic equation of the load is

$$\begin{cases} mx_q''(t) = -T \sin\theta_x(t) \cos\theta_y(t) \\ my_q''(t) = T \sin\theta_x(t) \sin\theta_y(t) \\ mz_q''(t) = T \cos\theta_x(t) - mg \end{cases} \quad (7)$$

After a series of processing of Equation (7), the expression of cable tension is obtained as

$$T = mg \cos\theta_x(t) + ml \cdot [\theta_x'^2(t) + \sin^2\theta_x(t) \cdot \theta_y'^2(t)] - mx_q''(t) \sin\theta_x(t) \cos\theta_y(t) + my_q''(t) \sin\theta_x(t) \cdot \sin\theta_y(t) + mz_q''(t) \cos\theta_x(t) - ml \quad (8)$$

### 4 Workspace analysis

The workspace of the multi-robot coordinated lifting system is defined as the set of all points of the position and pose that the load can reach under the condition of force and moment balance when the joint angle of the robot and the extension law of the cable are given (Li et al., 2015). To determine whether the load is in the workspace, it is only necessary to determine whether the cable tension satisfies the constrained condition.

#### 4.1 Static workspace analysis

The balance equation of the load is

$$J^T T = F \quad (9)$$

where  $T = [T_1 \ T_2 \ T_3]^T$ ,  $0 < T_{\min}^s \leq T_i \leq T_{\max}^s$ .  $F$  is the external force matrix of the load,

$$F = \left[ \left( m \frac{dv}{dt} \right)^T \left( [I_x \ I_y \ I_z] \frac{d\omega}{dt} \right)^T \right]^T \quad (10)$$

where  $I_x, I_y, I_z$  are the moment of inertia of the load, respectively,  $v$  and  $\omega$  are the linear and angular velocity of the load.

In Equation (9),  $J^T = [J_1 \ J_2 \ J_3]$  is the structure matrix of the lifting system:

$$J_i = \begin{bmatrix} e_i \\ (RB_i') \times e_i \end{bmatrix} \quad (i = 1, 2, 3) \quad (11)$$

where  $e_i = L_i / \|L_i\|$  is the unit vector of the cable length.

According to Equations (3) and (4), the cable length and load position of the lifting system can be calculated. The load position satisfies the following conditions:

$$\begin{cases} \min(x_1, x_2, x_3) < x < \max(x_1, x_2, x_3) \\ \min(y_1, y_2, y_3) < y < \max(y_1, y_2, y_3) \\ \min(z_1, z_2, z_3) < z < \max(z_1, z_2, z_3) \end{cases} \quad (12)$$

When the load pose is known, Equation (9) can be equivalent to in-homogeneous linear equations for solving the cable tension, and the condition  $\text{rank}(J) \leq \min(m, n)$  is satisfied.  $m=3$  is the number of cables, and  $n=6$  is the number of the load DOF. The static workspace of the lifting system is solved in the following steps.

(1) The end position of the robot and the load position are randomly generated by the Monte–Carlo algorithm. The rank ( $J$ ) and rank ( $J, F$ ) are separately calculated.

(2) We determine whether the  $\text{rank}(J) = \text{rank}(J, F) = m$  is true; if so, then  $T = J^{-1}F$ , and enter step (4); if not, we enter step (3).

(3) We determine whether  $\text{rank}(J) = \text{rank}(J, F) < m$  is true; if so, then  $T^* = J^T(JJ^T)^{-1}F$ , and enter step (4); if not, then return to step (1).

(4) We determine whether the cable tension  $0 < T_{\min}^s \leq T_i \leq T_{\max}^s$  is satisfied; if so, record the position of the point and enter step (5); if not, directly return to step (1).

(5) Repeating steps (1) to (4) until the cycle ends.

#### 4.2 Dynamic workspace analysis

When solving the dynamic workspace, the gravity and inertial forces of the load must be treated as the tension of the virtual cable to ensure that the lifting system satisfies the vector closure condition. In this case, the balance equation for the load is as follows:

$$J_s T_s = 0 \quad (13)$$

where  $J_s$  and  $T_s$  are the reconstructed structure and tension matrices of the lifting system. The solution steps for the dynamic workspace of the lifting system are as follows.



(1) The end position of the robot and the position of the load are randomly generated by the Monte–Carlo algorithm, and the structure matrix  $J_s^T$  is solved.

(2) Determine whether  $J_s^T$  has full rank; if so,  $T_{\text{eff}} = (J_s^T)^{-1}F$ , and enter step (3); if not, return to step (1).

(3) Calculate  $\lambda_1 = \max_{1 \leq i \leq m} \frac{T_{\text{min}} - T_{\text{eff}}(i)}{h_i}$  and  $\lambda_2 = \min_{1 \leq i \leq m} \frac{T_{\text{max}} - T_{\text{eff}}(i)}{h_i}$  and take the average value  $\lambda = (\lambda_1 + \lambda_2) / 2$ , then calculate  $T_{\text{nul}} = h\lambda$ ;  $h\lambda$  is a component of the null space matrix  $N(J_s^T)$ .

(4) Calculate the tension  $T = T_{\text{eff}} + T_{\text{nul}}$  and determine whether the cable tension  $0 < T_{\text{min}}^s \leq T_i \leq T_{\text{max}}^s$  is satisfied; if so, record the position of the point; if not, return to step (1).

(5) Repeat steps (1) to (4) until the cycle ends.

### 5 Numerical simulation analysis

The three floating robots are arranged in an equilateral triangle in space, and the ends of the three robots are kept at the same height. Figure 2 shows the projection of the lifting system in the initial state. Table 1 shows the initial positions of the barycenters and endpoints of the three floating robots. The structure of the floating base is a cylinder with height  $h = 1$  m and radius  $r = 0.5$  m. The parameters of the robot are  $a_1 = 1$  m,  $a_2 = 0.5$  m,  $a_3 = 0.5$  m, and the range of joint angles are shown in Table 2. The draft depth of the floating robot resting on the water surface is 0.5 m, the draft weight is 392.4 kg, and the fluid density is  $\rho = 10^3$  kg/m<sup>3</sup>. The mass of the load is 10 kg, the cable length is 0.5 to 3 m, and the initial position of the load is (1.5, 1.25, 1). The radius of the load is 0.1 m, the position of the connection points between the cables and the load are  $B_1 = [-0.05\sqrt{3}, -0.05, 0]^T$ ,  $B_2 = [0.05\sqrt{3}, -0.05, 0]^T$ , and  $B_3 = [0, 0.1, 0]^T$ .

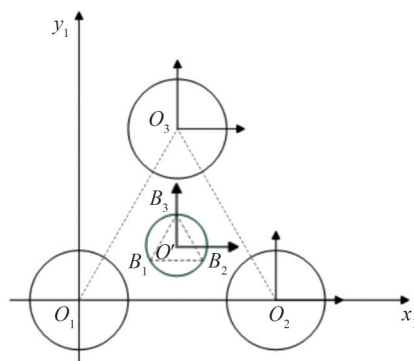


Figure 3 Projection of the lifting system on the XOY plane

#### 5.1 Simulation of the workspace

According to the established model of a multi-robot co-

Table 1 Initial coordinates of the floating robot

Points	X (m)	Y (m)	Z (m)
$O_1$	0	0	0
$O_2$	3	0	0
$O_3$	1.5	$1.5\sqrt{3}$	0
$A_1$	1	$5\sqrt{3}/6$	1.5
$A_2$	1	$-2\sqrt{3}/3$	1.5
$A_3$	7/4	$\sqrt{3}/12$	1.5

Table 2 Parameters of the joint angles

$\varphi_{11}$	$\varphi_{21}$	$\varphi_{31}$	$\varphi_{i2}, \varphi_{i3}$
$-\frac{\pi}{2} - \frac{\pi}{2}$	$\frac{\pi}{2} - \frac{3\pi}{2}$	$-\pi - 0$	$\frac{\pi}{12} - \frac{5\pi}{12}$

ordinated lifting system with a floating base, the driving pattern is such that the end positions of the robot and cable length change simultaneously. During the lifting, a random acceleration of 0–0.5 is added in the X, Y and Z directions of the load to obtain the dynamic workspace. Figures 4 and 5 show the static and dynamic workspace of the lifting system, where (a), (b), and (c) are the 3D projection diagram, respectively.

Figures 4 and 5 show that after  $3 \times 10^7$  random operations, the number of valid points in the static workspace is 184 140 and that in the dynamic workspace is 210 826. The number of valid points in the dynamic workspace is more than 10% of that in the static workspace. From the shape analysis, the basic shape of both workspaces is a triangular prism. As the load rises in the Z direction, the middle of the workspace is depressed, but the depression of the static workspace is more apparent than the dynamic workspace, given that the load has upward acceleration in the dynamic workspace, and together, the inertia force and cable tension balance the load gravity.

#### 5.2 Factors affecting the workspace

The shape and size of the workspace are important metrics to evaluate the performance of the floating multi-robot coordinated lifting system. Therefore, when the overall layout of the lifting system is carried out, the structural parameters or stress conditions of the system are changed to satisfy the parameter configuration under different conditions. The main factors that affect the workspace of the lifting system include the distribution position of the floating robot, external forces borne by the floating base, rod length and joint angle of the robot, maximum allowable tension of the cable, and the mass of the load. The external forces that can be borne by the floating base and the rod length and joint angle of the robot are the intrinsic features of the lifting system. The distributional position of the floating robot needs to be considered in combination with the actual working conditions and is not analyzed in this study. Only the maximum allowable tension of the cable and the load mass are analyzed.

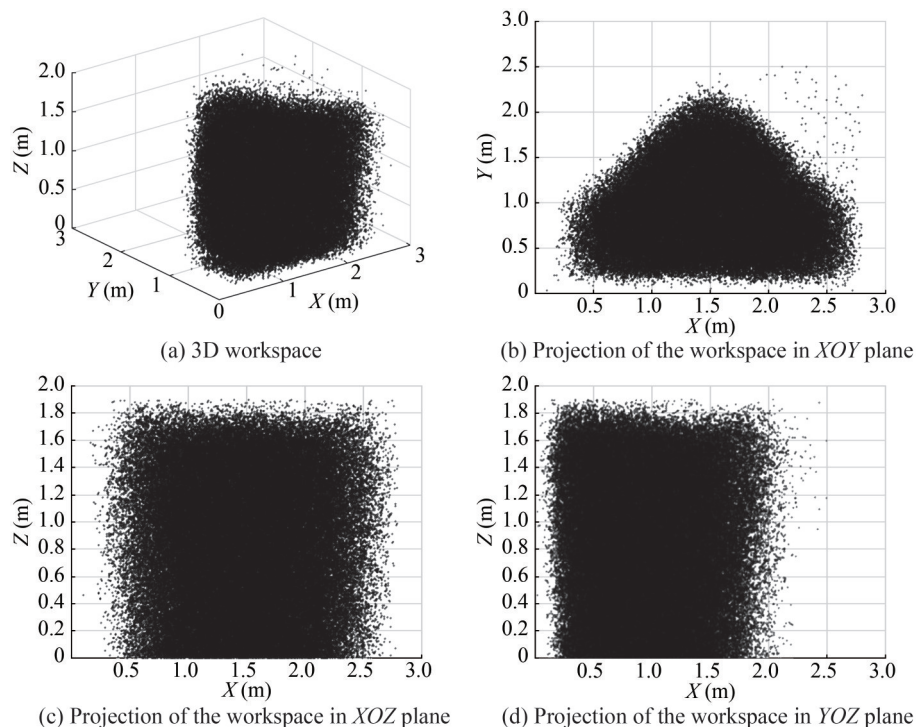


**Figure 4** Static workspace and 3D projection

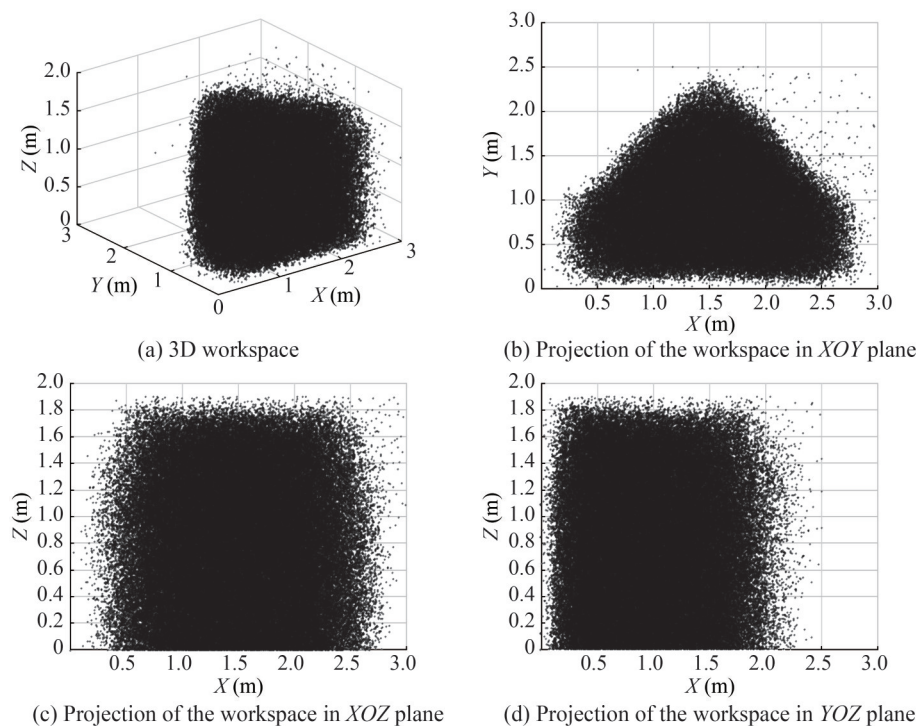


**Figure 5** Dynamic workspace and 3D projection

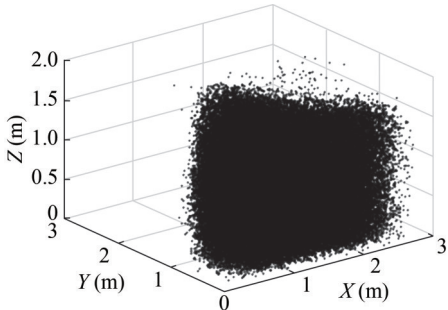
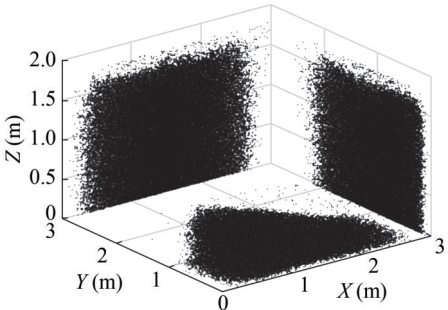
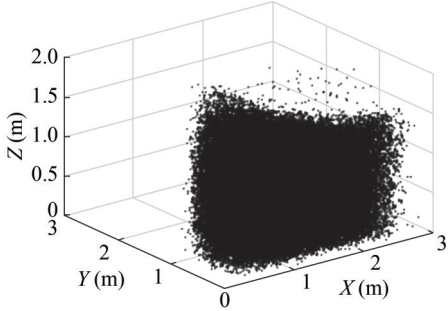
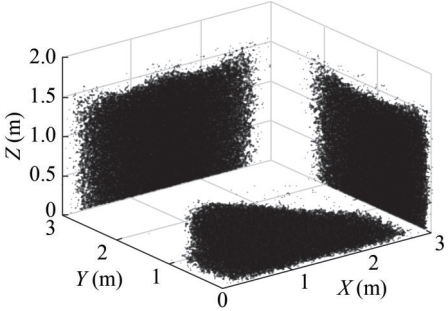
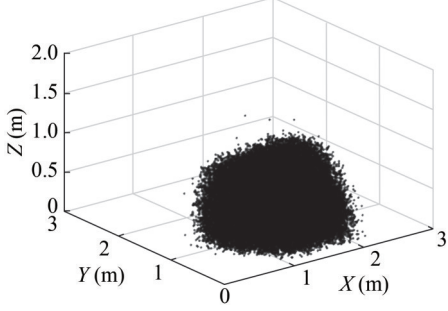
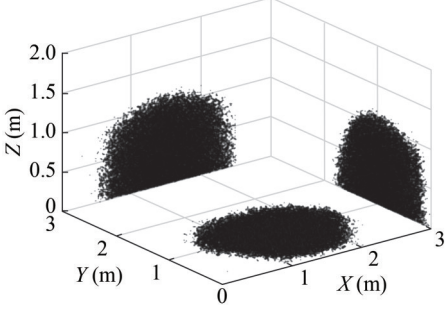
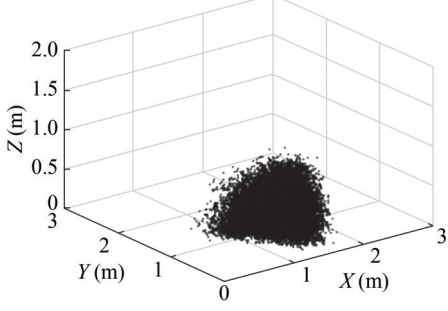
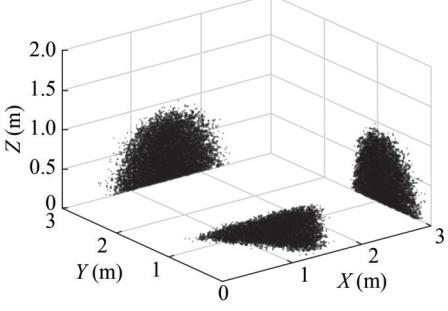
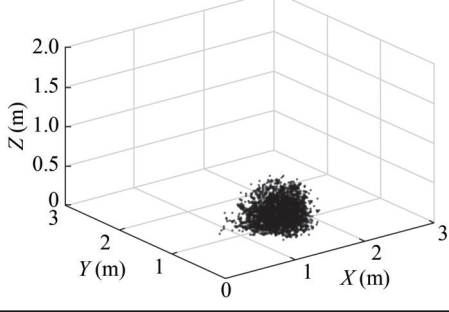
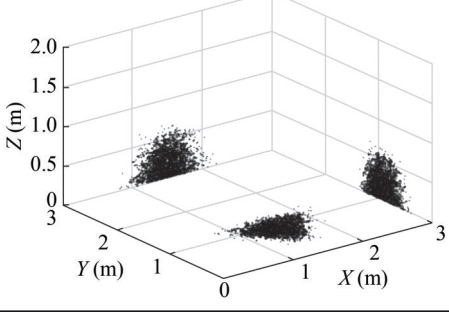
**5.2.1 Mass of the load**

The change in the load mass causes a change in the cable tension, although the characteristics of the cable itself do not change. The load mass directly changes the workspace of the lifting system. If the mass of the load is increased, the binding force of the cable on the load must be increased

to safely maintain the movement of the load. In practical applications, the lifting object at sea generally has a large mass. The mass range of the load must be limited, or a safe workspace must be made to perform the lifting operation safely and reliably. Table 3 shows the static and dynamic workspaces for different load masses.

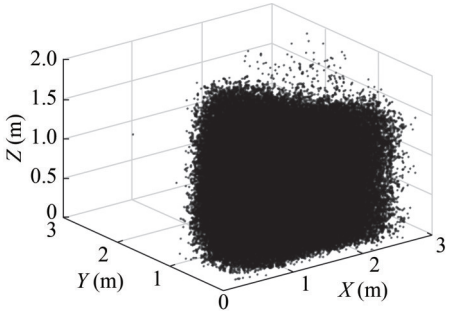
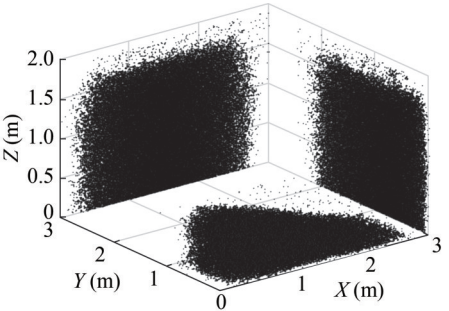
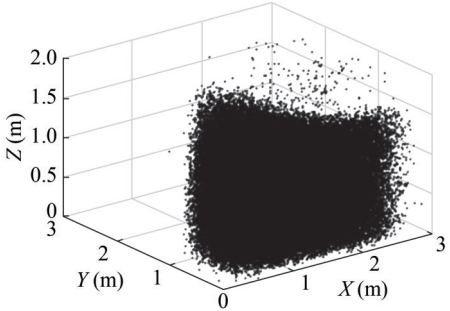
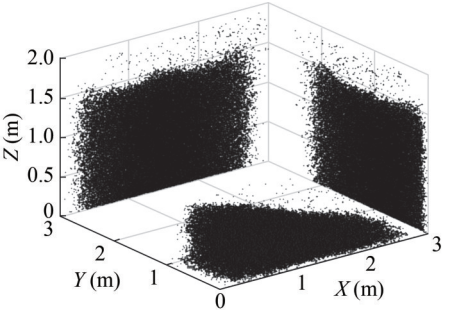
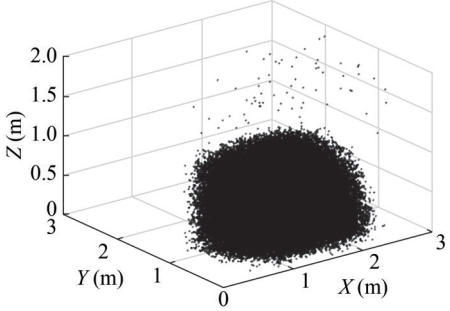
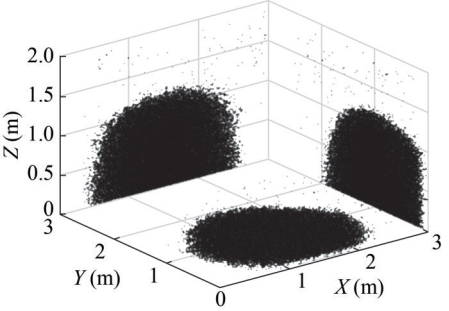
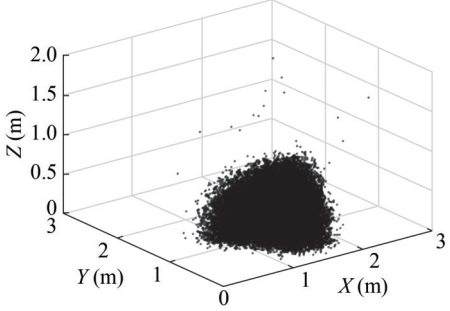
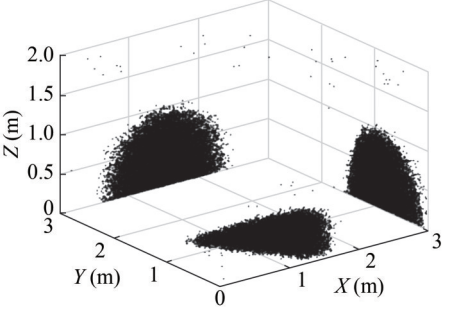
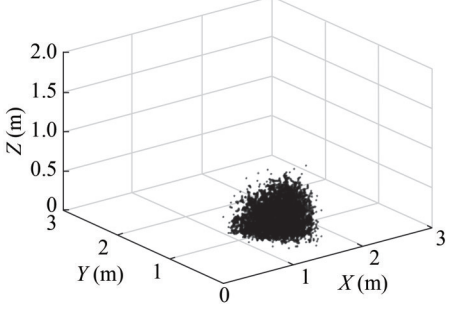
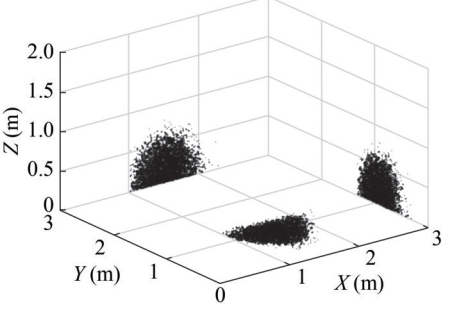
**Table 3** Workspace and 3D projection diagram for different load masses

(a) Static workspace

Load mass (kg)	Workspace	3D projection diagram	Valid points
20			175 780
35			147 360
50			12 728
65			17 435
80			2 575

**Table 3** Workspace and 3D projection diagram for different load masses (continuous)

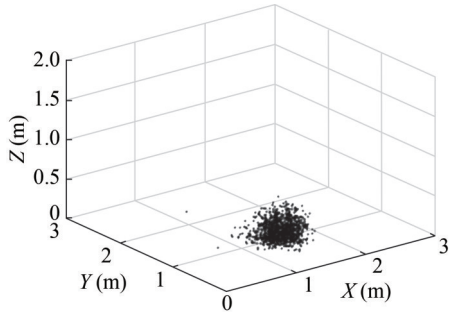
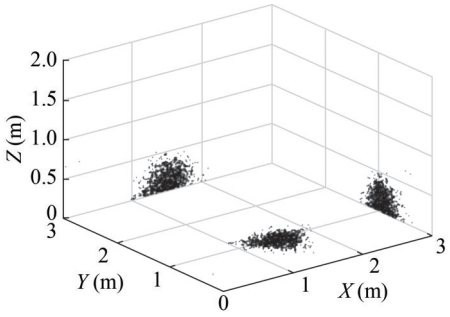
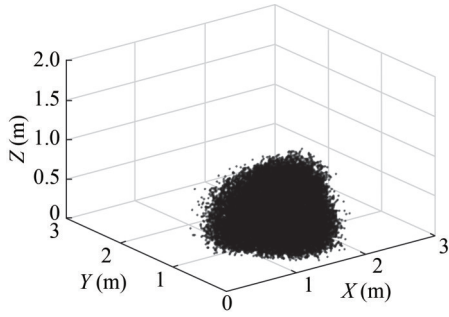
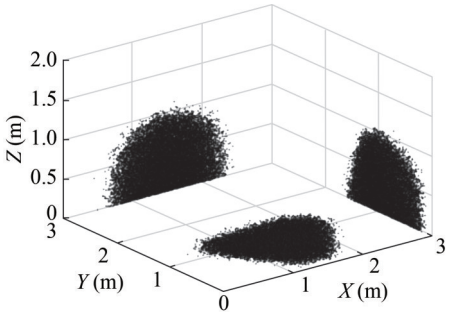
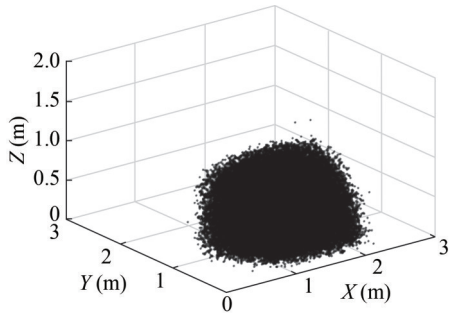
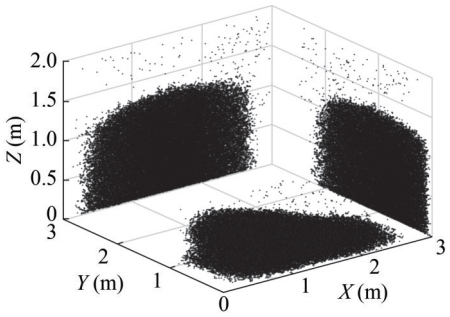
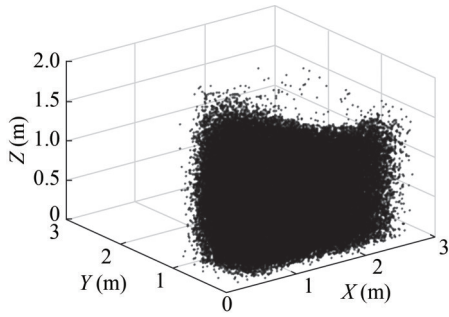
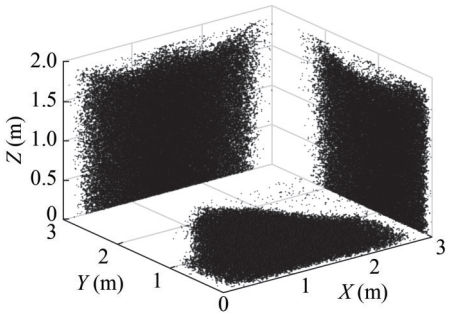
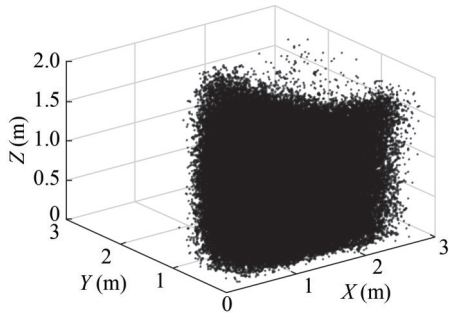
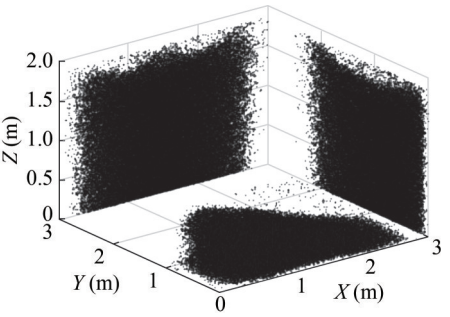
(b) Dynamic workspace

Load mass (kg)	Workspace	3D projection diagram	Valid points
20			188 855
35			169 915
50			107 703
65			33 168
80			4 537



**Table 4** Workspace and 3D projection diagram for different maximum allowable tensions of the cable

(a) Static workspace

Cable tension (N)	Workspace	3D projection diagram	Valid points
50			976
70			38 965
90			81 960
150			151 048
300			191 833

**Table 4** Workspace and 3D projection diagram for different maximum allowable tensions of the cable (continuous)

(b) Dynamic workspace

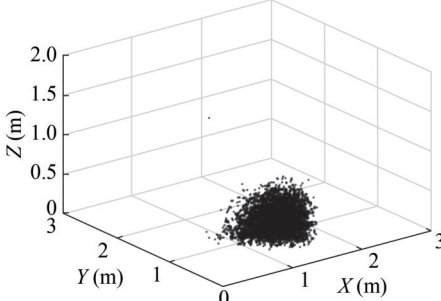
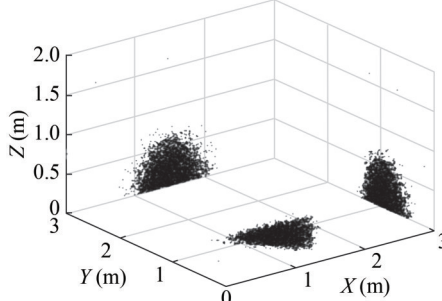
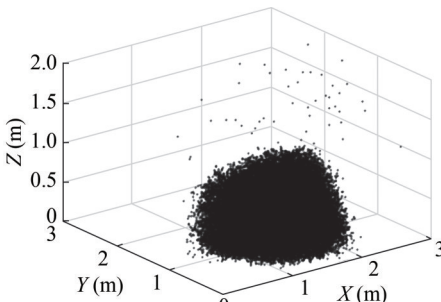
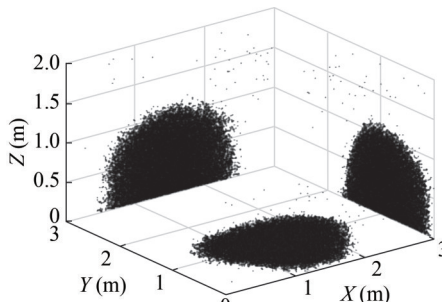
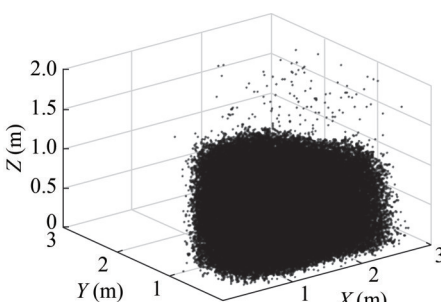
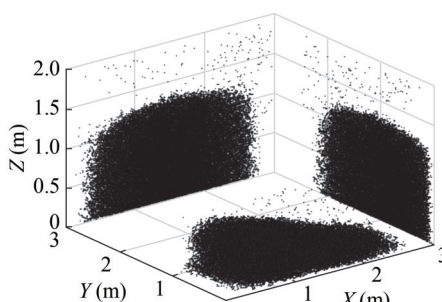
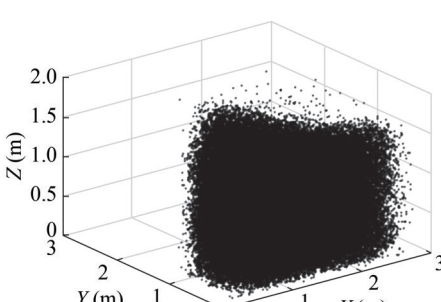
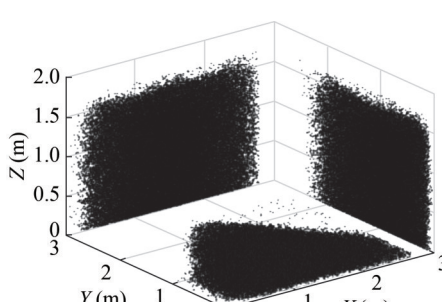
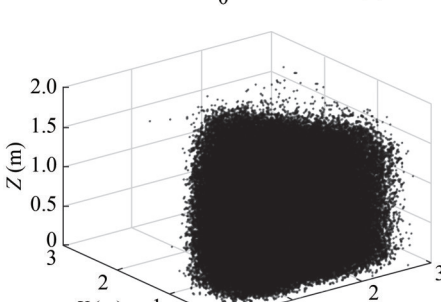
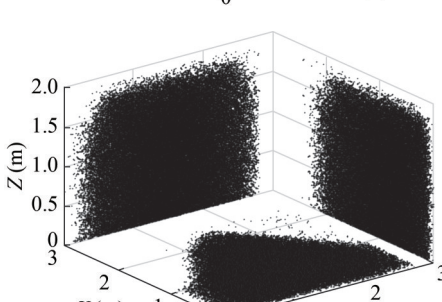
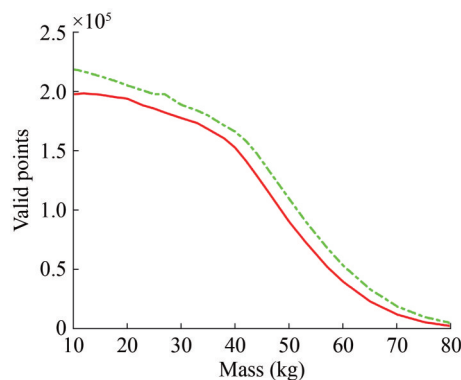
Cable tension (N)	Workspace	3D projection diagram	Valid points
50			4 671
70			65 438
90			142 066
150			168 940
300			213 711

Table 3 shows that as the load mass increases, the height of the workspace gradually decreases, and the top of the workspace depresses downward. The shape of the workspace depresses downward. The shape of the workspace with a load mass of less than 50 kg is a triangular prism. When the load mass is greater than 50 kg, the top of the workspace protrudes upward, the *XOY* projection plane gradually changes from a regular triangle to an ellipse, and the shape of the workspace changes from a half-sphere to a triangular pyramid.

In Figure 6, the red and green curves indicate the static and dynamic workspaces of the lifting system, respectively. The figure shows that the number of valid points in the dynamic workspace is larger than that in the static workspace at any load mass. When the load mass is less than 40 kg, the number of valid points in both workspaces slowly decreases. When the load mass is 40–60 kg, the number of valid points in the workspace decreases rapidly, and when the load mass exceeds 80 kg, the reduction rate decreases. Therefore, considering the safe height of different loads in the workspace under practical working conditions is necessary.



**Figure 6** Valid points of the workspace for different load mass

### 5.2.2 Maximum allowable tension of the cable

A reasonable distribution of the cable tension in the multi-robot coordinated lifting system is important. The cables must always be kept tight during the load movement, and to ensure a uniform distribution of tension, the three cables must be limited to a minimum preload to avoid the spurious strain of the load. Similarly, the maximum allowable tension of the cable must also be limited. Table 4 shows the static and dynamic workspaces for different maximum allowable tensions of the cable.

Table 4 shows that as the maximum allowable tension of the cable increases, the number of valid points of the two workspaces increases. The shape of the workspace gradually changes from a triangular pyramid to a half-sphere and finally to a triangular prism. The cable tension gradually increases, and the shape of the workspace in the *XOY* projection plane changes from an inverted to an equilateral triangle. The increase in cable tension mainly changes the workspace height.

In Figure 6, the red and green curves indicate the static and dynamic workspaces of the lifting system, respectively. From Figure 7, we can conclude that the shape of the workspace changes considerably when the cable tension is less than 150 N, but changes little when it is greater than 150 N. The cable tension mainly balances the load gravity. When the maximum allowable tension of the cable increases, the workspace gradually increases from bottom to top. Meanwhile, when the minimum preload force of the cable increases, the working space gradually decreases from bottom to top.

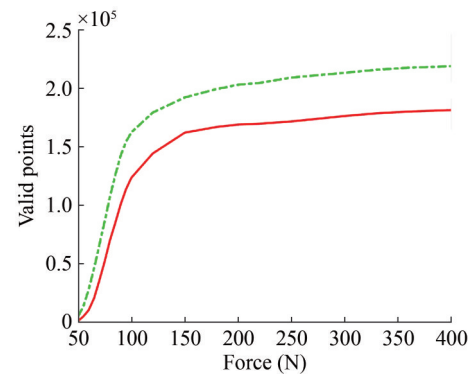


**Figure 7** Valid points of the workspace for different maximum allowable tensions of the cable

In summary, when a single lifting robot is unable to meet the lifting requirements, multiple robots can be used to achieve the task. As multiple robots work, the force on the load gradually increases in the horizontal direction, which reduces the swing of the load.

## 6 Conclusions

This study examined the kinematics, dynamics and workspace of the lifting system. The main content and conclusions are as follows:

- 1) The kinematics and dynamics of the lifting system are analyzed, and the constraints that the load should meet in the workspace are obtained.
- 2) Based on the virtual cable and closed principle of the force-spinor, the calculated steps of the workspace of the lifting system are determined by the Monte–Carlo algorithm.
- 3) The influence of load mass and maximum allowable tension of cables on static workspace and dynamic workspace are analyzed, which provides guidance for the practical application of the lifting system.

The floating multi-robot coordinated lifting system presents considerable potential in practical applications. In this study, the Monte–Carlo algorithm is used to solve the workspace of the lifting system; however, the boundary of the workspace is not clear enough and needs further study.

**Funding** Supported by the National Natural Science Foundation of China under Grant No. 51965032, the National Natural Science Foundation of Gansu Province of China under Grant No. 22JR5RA319, the Science and Technology Foundation of Gansu Province of China under Grant No. 21YF5WA060, and the Excellent Doctoral Student Foundation of Gansu Province of China under Grant No. 23JRRA842.

**Competing interest** The authors have no competing interests to declare that are relevant to the content of this article.

## References

- Bedoustani YB, Taghirad HD, Aref MM (2009) Dynamics analysis of a redundant parallel manipulator driven by elastic cables. *International Conference on Control*, 1-6
- Bisgaard M, Bendtsen JD, Habbo AL (2009) Modeling of generic slung load system. *Journal of Guidance, Control, and Dynamics* 32(2): 573-585. DOI: 10.2514/1.36539
- Bisgaard M, Habbo AL, Bendtsen JD (2010) Adaptive control system for autonomous helicopter slung load operations. *Control Engineering Practice* 18(7): 800-811. DOI: 10.1016/j.conengprac.2010.01.017
- Boscher P, Ebertuphoff I, Riechel AT (2006) Wrench-feasible workspace generation for cable-driven robots. *IEEE Transactions on Robotics* 22(5): 890-902. DOI: 10.1109/tro.2006.878967
- Cong BP, Song HY, Yang G (2005) Dynamic analysis of cable driven parallel mechanisms. *IEEE/ASME International Conference on Advanced Intelligent Mechatronics*, 1-8
- Chen RJ, Wu ZW, Wang T (2001) Modeling and analysis for agent-based distributed multiple robot system. *China Mechanical Engineering* 12(6): 667-671. (in Chinese) DOI: 10.3321/j.issn:1004-132X.2001.06.017
- Chen Y, Jiang Y, Tang L (2020) Dynamic modeling of 4-DOF cable-driven rigid-flexible hybrid wave motion compensation mechanism. *Journal of Central South University* 51(7): 1767-1780. DOI: 10.1007/s12206-020-0415-x
- Craig, John J, Yun C (2018) *Introduction to robotics*. Machinery Industry Press, Beijing, 76-88
- Ding HF, Qian S, Zi B (2012) Design and analysis of cooperative cable parallel manipulators for multiple mobile cranes. *International Journal of Advanced Robotic Systems* 9(5): 56-61. DOI: 10.5772/53670
- Diao X, Ou M (2007) A method of verifying force-closure condition for general cable manipulators with seven cables. *Mechanism & Machine Theory* 42(12): 1563-1576. DOI: 10.1016/j.mechmachtheory.2007.06.008
- Guan Y, Yokoi K (2006) Reachable space generation of a humanoid robot using the Monte Carlo method. *IEEE International Conference on Intelligent Robots and Systems*, 1-9
- Horoub MM, Hassan M (2018) Influence of cables layout on the dynamic workspace of a six-DOF parallel marine manipulator. *Mechanism and Machine Theory* 129: 191-201. DOI: 10.1016/j.mechmachtheory.2018.07.022
- Horoub MM, Hassan M, Hawwa MA (2017) Workspace analysis of a Gough-Stewart type cable marine platform subjected to harmonic water waves. *Mechanism and Machine Theory* 120: 314-325. DOI: 10.1016/j.mechmachtheory.2017.09.001
- Idres MM, Mook D, Youssef KS (2003) A nonlinear 8-DOF coupled crane-ship dynamic model. *Structural Dynamics and Materials Conference, Norfolk, USA*, 1-5
- Jia N, Qian S, Yang SG (2015) Design and feasibility study of connecting device for cooperation of multiple mobile cranes. *Machinery Design & Manufacture* 1(7): 200-203. (in Chinese) DOI: 10.19356/j.cnki.1001-3997.2015.07.055
- Li JH (2021) *Workspace and stability analysis of coordinated lifting system for floating multi-robot*. Master thesis, Lanzhou Jiaotong University, Lanzhou, 30-45
- Li W, Su C, Ye JN (2015) Analysis of dynamic workspace for under-constrained coordinate suspending system with multi-robots. *Journal of Shanghai Jiao Tong University* 49(10): 1916-1923. (in Chinese) DOI: 10.16183/j.cnki.jsjtu.2019.02.014
- Liu HT, Xu K, Yue W (2021a) Kinematics modeling and optimal design of a partially compliant four-bar linkage using elliptic integral solution. *Mechanism and Machine Theory* 157: 1-15. DOI: 10.1016/j.mechmachtheory.2020.104214
- Liu XF, Tang YH, Liu X (2021b) Dynamic performance optimization for redundantly actuated parallel manipulator with constraint branch. *Transactions of the Chinese Society for Agricultural Machinery* 52(8): 378-385. (in Chinese) DOI: 10.6041/j.issn.1000-1298.2021.05.042
- Qian S, Zi B, Zhang D (2014) Kinematics and error analysis of cooperative cable parallel manipulators for multiple mobile cranes. *International Journal of Mechanics & Materials in Design* 10(4): 395-409. DOI: 10.1007/s10999-014-9250-5
- Qian S, Zi B, Zhou B (2017) Dynamic modeling and analysis of cable parallel manipulator for dual automobile cranes during luffing motion. *Journal of Mechanical Engineering* 53(7): 55-61. (in Chinese) DOI: 10.3901/JME.2017.07.055
- Ren HL (2008) *Study on rigid-flexible coupling dynamic modeling and dynamic characteristics of mooring crane*. PhD thesis, Huazhong University of Science and Technology, Wuhan, 20-25
- Schellin TE, Jiang T, Sharma SD (1991) Crane ship response to wave groups. *Journal of Offshore Mechanics and Arctic Engineering* 113(3): 211-218. DOI: 10.1115/1.2919922
- Su C, Wang ZR, Zhao ZG (2021) Dynamic response simulation analysis of floating base multi-robot coordinated lifting system. *Journal of Vibration and Shock* 40(23): 232-238. (in Chinese) DOI: 10.13465/j.cnki.jvs.2021.23.031
- Tang XQ, Tang LW, Wang J (2013) Workspace quality analysis and application for a completely restrained 3-DOF planar cable-driven parallel manipulator. *Journal of Mechanical Science and Technology* 27(8): 2391-2399. DOI: 10.1007/s12206-013-0624-7
- Verhoeven R, Hiller M (2000) Estimating the controllable workspace of tendon-based Stewart platforms. *Advances in Robot Kinematics*, 88-96
- Wang GX, Yuan DN, Liu HZ (2012) Kinematic analysis of spatial 4-SPS/CU parallel mechanism. *Transactions of the Chinese Society for Agricultural Machinery* 43(3): 207-212. (in Chinese) DOI: 10.6041/j.issn.1000-1298.2012.03.037
- Yu XB, He W, Li Q, Li YN, Li B (2021) Human-robot co-carrying using visual and force sensing. *IEEE Transactions on Industrial Electronics* 68(9): 8657-8666. DOI: 10.1109/TIE.2020.3016271
- Yu XB, Li B, He W, Feng YH, Cheng L, Silvestre C (2022) Adaptive-constrained impedance control for human-robot co-transportation. *IEEE Transactions on Cybernetics* 52(12): 13237-13249. DOI: 10.1109/TCYB.2021.3107357